



HAL
open science

Calcium signalling-dependent mitochondrial dysfunction and bioenergetics regulation in respiratory chain Complex II deficiency

Mounia Chami, Eleonore Mbaya-Moutula, Bénédicte Oulès, Casper Caspersen, Rachida Tacine, Hélène Massinet, Dominique Chrétien, Arnold Munnich, Agnes Rotig, Rosario Rizzuto, et al.

► To cite this version:

Mounia Chami, Eleonore Mbaya-Moutula, Bénédicte Oulès, Casper Caspersen, Rachida Tacine, et al.. Calcium signalling-dependent mitochondrial dysfunction and bioenergetics regulation in respiratory chain Complex II deficiency. *Cell Death and Differentiation*, 2010, 10.1038/cdd.2010.51 . hal-00538097

HAL Id: hal-00538097

<https://hal.science/hal-00538097>

Submitted on 21 Nov 2010

HAL is a multi-disciplinary open access archive for the deposit and dissemination of scientific research documents, whether they are published or not. The documents may come from teaching and research institutions in France or abroad, or from public or private research centers.

L'archive ouverte pluridisciplinaire **HAL**, est destinée au dépôt et à la diffusion de documents scientifiques de niveau recherche, publiés ou non, émanant des établissements d'enseignement et de recherche français ou étrangers, des laboratoires publics ou privés.

Calcium signalling-dependent mitochondrial dysfunction and bioenergetics regulation in respiratory chain Complex II deficiency

Eléonore MBaya^{1, 2#}, Bénédicte Oulès^{1, 2#}, Casper Caspersen^{1, 2}, Rachida Tacine^{1, 2}, Hélène Massinet^{1, 2}, Maria Pennuto⁶, Dominique Chrétien^{2, 3}, Arnold Munnich^{2, 3}, Agnès Rötig^{2, 3}, Rosario Rizzuto⁴, Guy A. Rutter⁵, Patrizia Paterlini-Bréchet^{1, 2} and Mounia Chami^{1, 2, 6}.

¹INSERM U 807, Paris, F-75015 France; ²Paris V University, Paris, F-75015, France; ³INSERM U 781, Paris, F-75015 France; ⁴Department of Experimental and Diagnostic Medicine, Section of General Pathology, University of Ferrara, 44100, Italy; ⁵Section of Cell Biology, Division of Medicine, Faculty of Medicine, Imperial College London, London SW72AZ, United Kingdom. ⁶The Italian Institute of Technology, Via Morego, 30, 16163, Genova, Italy.

Running title: Complex II defect-mediated calcium deregulation

Address correspondence to: Mounia Chami, The Italian Institute of Technology, Via Morego 30, 16163, Genova, Italy. Tel: 00.39.01071781566, Email: mounia.chami@iit.it

Mbaya E. and Oulès B. contributed equally to this work

Abstract

Despite advanced knowledge on the genetic basis of oxidative phosphorylation (OXPHOS)-related diseases, the molecular and/or cellular determinants for tissue specific dysfunction are not completely understood. Here, we report the cellular events associated with mitochondrial respiratory Complex II deficiency occurring prior to cell death. Mutation or chronic inhibition of Complex II determined a large increase of basal and agonist-evoked Ca^{2+} signals in the cytosol and the mitochondria, in parallel with mitochondrial dysfunction characterized by membrane potential ($\Delta\psi_{\text{mit}}$) loss, [ATP] reduction and increased Reactive Oxygen Species (ROS) production. cytosolic and mitochondrial Ca^{2+} overload are linked to increased ER Ca^{2+} leakage, and to SERCA2b and PMCA proteasome-dependent degradation. Increased $[\text{Ca}^{2+}]_{\text{mit}}$ is also contributed by decreased mitochondrial motility and increased ER-mitochondria contact sites. Interestingly, increased intracellular $[\text{Ca}^{2+}]$ activated on the one hand a compensatory Ca^{2+} -dependent glycolytic ATP production and determined on the second hand mitochondrial pathology. These results revealed the primary role for Ca^{2+} signalling in the control of mitochondrial dysfunction and cellular bioenergetics outcomes linked to respiratory chain Complex II deficiency.

Keywords: Mitochondria, respiratory chain pathologies, calcium, bioenergetics, SERCA, PMCA, proteasome, cell death.

Abbreviation list: Ca^{2+} : Calcium; Cyt: cytosol; $[\text{Ca}^{2+}]_{\text{cyt}}$: cytosolic free Ca^{2+} concentration; ER, endoplasmic reticulum; $[\text{Ca}^{2+}]_{\text{er}}$: endoplasmic reticulum Ca^{2+} concentration; $[\text{Ca}^{2+}]_{\text{mit}}$: mitochondrial free Ca^{2+} concentration; IP_3 : inositol 1, 4, 5-triphosphate; $\Delta\psi_{\text{m}}$: mitochondrial potential; $[\text{ATP}]_{\text{mit}}$: mitochondria ATP free concentration; OXPHOS: oxidative phosphorylation; PMCA: Plasma membrane Ca^{2+} ATPase; ROS: reactive oxygen species; SERCA2: Sarco-Endoplasmic Reticulum Ca^{2+} ATPase 2; SDHA: succinate dehydrogenase A subunit.

Introduction

Mitochondria are the driving force behind life, as mitochondrial oxidative phosphorylation provides the main source of ATP in the cell. In addition to energy production, mitochondria play a crucial role in mediating amino acid biosynthesis, fatty acid oxidation, intermediate metabolic pathways, free radicals production and scavenging and Ca^{2+} homeostasis (1).

Mitochondria affect intracellular Ca^{2+} metabolism in two ways: i) directly by regulating both the amplitude, duration, location and propagation of cytosolic Ca^{2+} elevations and the recycling of Ca^{2+} towards the ER (2); ii) indirectly by producing ATP which is used by Ca^{2+} -dependent ATPases to pump Ca^{2+} out of the cell (by the plasma-membrane Ca^{2+} ATPase: PMCA) or into intracellular stores (by the sarco-endoplasmic reticulum Ca^{2+} ATPase: SERCA). Conversely Ca^{2+} entering to the mitochondrial matrix regulates mitochondrial metabolism through the activation of the Ca^{2+} -dependent enzymes of the Krebs cycle (3).

Leigh's syndrome is a rare (1/36,000 births) but severe and fatal encephalopathy of early childhood that is most frequently associated with deficiencies in nucleus-encoded subunits of Complex I (NDUFS3 and NDUFS7) (4, 5), Complex II (SDHA) (6), Complex IV (SURF1) (7) or pyruvate dehydrogenase (8). Despite the identification of the genetic origin of Leigh's syndrome, the molecular and cellular events associated with pathology are not completely understood.

Deregulations of intracellular Ca^{2+} signalling have been reported in different models of mitochondrial respiratory chain diseases and the most studied ones are those related to mitochondrial DNA mutations (9, 10) and nuclear DNA mutations affecting Complex I (11), while data on Complex II deficiency are still lacking.

Complex II (succinate: ubiquinone oxidoreductase) plays a central role in oxidative metabolism, being a key enzyme of the citric acid cycle as well as a Complex of the mitochondrial respiratory chain (12).

We report here the cellular events deriving from Complex II mutation associated with Leigh's syndrome. The study was conducted both in human derived mutated fibroblasts and in cellular models in which we mimicked Complex II deficiency by using Complex II inhibitors. We showed broad subcellular Ca^{2+} signalling alterations occurring prior to cell demise in Complex II deficient cells. Interestingly, we showed that cytosolic and mitochondrial Ca^{2+} overload are linked to SERCA and PMCA degradation occurring in a

proteasome-dependent manner. Our study revealed a dual role of Ca^{2+} deregulation in the control of cellular bioenergetics outcome and mitochondrial pathology.

Results

We studied fibroblasts isolated from a patient with Leigh's syndrome harbouring a homozygous Arg554Trp substitution in the Fp subunit of the Complex II (SDHA_{R554W}) (13). These fibroblasts were shown to harbour a reduction of Complex II activity to ~ 30 % of control values in the absence of cell death (14). Leigh's syndrome associated with Complex II mutations was described in very rare cases (6). To bypass this limitation, we conducted the whole study in parallel with two inhibitors of Complex II. We thus used fibroblasts derived from healthy individuals and the neuronal derived cell line (SH-SY5Y) left untreated or treated with Complex II inhibitors: 3-NP (3-nitropropionic acid) or Atpenin A5 (15, 16). 3-NP is structurally similar to Complex II substrate succinate thus interacting with some residue in the active site of the enzyme (15). Atpenins were shown to share structural similarity with Ubiquinone (UQ) thus blocking the electron transfer between the enzyme and UQ by binding to a region that partly overlaps with the physiological UQ-binding site (16). To note, we deliberately used: i) concentrations of 3-NP (300 μ M) and Atpenin A5 (100 nM) which did not induce cell death at 20 h thus affording to study Complex II deficiency independently from cell death (Supplementary Figure S1a); and ii) extended application (20 h) of the drugs in order to chronically inhibit Complex II (Supplementary Figure S1b). Importantly, Complex II activity was reduced to 15-40 % of control values in both mutated cells and control fibroblasts and SH-SY5Y cells treated with 300 μ M 3-NP and 100 nM Atpenin A5 for 20 h (Supplementary Figure S1b and Table S1). Finally, we show that application of 300 μ M 3-NP or 100 nM Atpenin A5 for 72 h or 1 mM 3-NP for 20 h determined cell death demonstrating that complex II inhibition is linked to cell death (Supplementary Figure S1c and 1d right).

In order to demonstrate that in our conditions we mimicked chronic Complex II inhibition upon drug application, we measured Complex II activity at 6 h and 20 h after treatment with 300 μ M 3-NP. Interestingly, reduction of Complex II activity occurred upon 6 h of treatment and was maintained to a similar level upon 20 h of treatment (data not shown).

We assessed mitochondrial functionality upon Complex II mutation or inhibition. Mitochondrial potential ($\Delta\psi_{mit}$) was measured by using TMRM dye which accumulates within the mitochondrial matrix as a function of $\Delta\psi_{mit}$. As expected, we observed a significant decrease (~ 70 % vs control considered as 100 %) of $\Delta\psi_{mit}$ (normalized TMRM signal) upon Complex II mutation or inhibition in both fibroblasts and SH-SY5Y cells (Figure 1a and 1b respectively and Supplementary Table S2).

The mitochondrial respiratory chain is known to be the major source of Reactive Oxygen Species (ROS) within the cell. Moreover, it has been shown that ROS can stimulate mitochondrial uncoupling and that the processes of uncoupling and ROS generation exist in a feedback loop (17). We thus measured mitochondrial production of superoxide ($O_2^{\cdot-}$) by using MitoSOX red mitochondrial superoxide indicator (18). Complex II mutated cells displayed an increase in mitochondrial $O_2^{\cdot-}$ production of almost 25 % as compared to control (Figure 1c and Supplementary Table S3). A similar result was also observed upon chronic application of Complex II inhibitors. The specificity of the test was confirmed by using the ROS scavenger pyrrolidine dithiocarbamate (PDCT) (Figure 1c and Supplementary Table S3). This result is consistent with previously reported data which show increased activities of both mitochondrial and cytosolic inducible superoxide dismutase in $SDHA_{R554W}$ cells (19).

Next, we sought to analyze the impact of the mitochondrial Complex II defect on ATP level. Basal mitochondrial ATP concentration ($[ATP]_{mit}$) was measured using a luciferase probe targeted to the mitochondria (mitLuc) (20). We observed a decreased basal $[ATP]_{mit}$ in $SDHA_{R554W}$ mutated fibroblasts (74 % of that in control cells) as well as in SH-SY5Y cells upon chronic Complex II inhibition (83 % in 3-NP, and 77 % in Atpenin A5 of that in control cells) (Figure 1d and 1e, and Supplementary Table S4).

Ca^{2+} is a key regulator of mitochondrial function and acts at several levels within the organelle to stimulate OXPHOS (3). We thus measured subcellular Ca^{2+} signalling in fibroblasts and SH-SY5Y cells upon Complex II mutation or inhibition. Measurement of basal $[Ca^{2+}]_{cyt}$, by using the Fluo-4,AM dye, revealed a significant increase (~ 2 to 4 fold) of basal $[Ca^{2+}]_{cyt}$ in $SDHA_{R554W}$ mutated fibroblasts and in control fibroblasts upon Complex II inhibition as compared to non-treated ones (Figure 2a and Supplementary Table S5). Similarly, we also observed an increase of basal $[Ca^{2+}]_{mit}$ in $SDHA_{R554W}$ mutated fibroblasts and in control fibroblasts upon Complex II inhibition (~ 1.5 to 2 fold) as compared to non-treated cells as measured by X-Rhod-1, AM probe (Figure 2b and Supplementary Table S6).

We then analyzed agonist-evoked cytosolic and mitochondrial Ca^{2+} signals using adenovirus-delivered recombinant aequorin Ca^{2+} probes (cytAEQ, mitAEQ respectively).

By using the cytosolic aequorin probe, we first showed a significant increase (~ 1.5 to 1.7 fold) of the agonist-evoked cytosolic Ca^{2+} signal ($[Ca^{2+}]_{cyt}$) in $SDHA_{R554W}$ mutated fibroblasts and SH-SY5Y cells upon Complex II inhibition as compared to controls (Figure 2c, and Supplementary Table S7).

By using the mitochondrial aequorin probe, we also noticed a significant increase of agonist-evoked mitochondrial Ca^{2+} signal ($[\text{Ca}^{2+}]_{\text{mit}}$) in $\text{SDHA}_{\text{R554W}}$ mutated fibroblasts (~ 3 fold increase) and SH-SY5Y cells upon Complex II inhibition (~ 1.5 fold increase) as compared to controls (Figure 2d and Supplementary Table S8).

Mitochondrial Ca^{2+} uptake and $\Delta\psi_{\text{mit}}$ are tightly cross-regulated (1). On the one hand, the main driving force for Ca^{2+} accumulation across the inner mitochondrial membrane is the electrochemical gradient ($\Delta\mu\text{H}$) established and maintained by the respiratory chain, while, on the other hand, depolarization occurs transiently following Ca^{2+} uptake in physiological conditions (21). We thus measured the kinetics of the Ca^{2+} and potential changes occurring in mitochondria of Complex II deficient cells. Interestingly, we observed an increased agonist-evoked mitochondrial Ca^{2+} response as early as after 4 h of treatment with Complex II inhibitors. Increased mitochondrial Ca^{2+} signal was also seen after 6 h of treatment (Figure 3a and Supplementary Table S8). This result was observed with both inhibitors 3-NP and Atpenin A5 and in both fibroblasts and SH-SY5Y cells (Figure 3a and Supplementary Table S8). In parallel, no modification of $\Delta\psi_{\text{mit}}$ was noticed in cells treated in the same conditions as for Ca^{2+} analyses (Figure 3b and Supplementary Table S2). This result suggests that increase of mitochondrial Ca^{2+} uptake precedes the loss of $\Delta\psi_{\text{mit}}$ in Complex II deficient cells.

We then investigated the mechanisms underlying increased $[\text{Ca}^{2+}]$ associated with Complex II deficiency. Since cytosolic and mitochondrial Ca^{2+} signals are largely contributed by the endoplasmic reticulum (ER) Ca^{2+} store, we measured the state of ER Ca^{2+} load by using the ER targeted aequorin probe. Mutation of the SDHA subunit was shown to induce a decrease of steady state ER free Ca^{2+} ($[\text{Ca}^{2+}]_{\text{ER}}$) by almost ~ 40 % as compared to three different controls (Figure 4a and Supplementary Table S9). A slighter but significant decrease (~ 15 %) of ER steady state was also obtained upon Complex II inhibition by 3-NP and Atpenin A5 (Supplementary Figure S2a and Table S9). We then demonstrated that the decreased $[\text{Ca}^{2+}]_{\text{ER}}$ is associated with decreased ER Ca^{2+} uptake rate, and increased passive ER Ca^{2+} leakage (Figure 4b and 4c respectively). No modification of agonist-evoked Ca^{2+} release from the store was noticed between control and Complex II deficient cells (Supplementary Figure S2b).

Previous data have shown that ER Ca^{2+} depletion can be linked to the induction of the unfolded protein response (UPR) (22). However, our data revealed no induction of UPR in $\text{SDHA}_{\text{R554W}}$ cells (Supplementary Figure S3).

Finally, no clear modification of capacitative Ca^{2+} entry was noted in $\text{SDHA}_{\text{R554W}}$ mutated cells as compared to controls (Figure 4d) ruling out a change in Ca^{2+} influx in the observed $[\text{Ca}^{2+}]_{\text{cyt}}$ and $[\text{Ca}^{2+}]_{\text{mit}}$ increase.

These results may indicate that the increased cytosolic and mitochondrial agonist-evoked Ca^{2+} signals are largely contributed by increased basal Ca^{2+} levels. This late event is a likely due, at least in part, to decreased ER Ca^{2+} store load and increased ER Ca^{2+} emptying through increased Ca^{2+} leak.

In order to decipher the molecular mechanisms underlying the intracellular Ca^{2+} overload related to Complex II deficiency, we next analyzed SERCA and PMCA expression by western blotting. SH-SY5Y cells are known to express mostly SERCA2b and PMCA2 isoforms. As shown in Figure 5a, a significant decrease of SERCA2b and PMCA2 expression was observed in $\text{SDHA}_{\text{R554W}}$ cells and in SH-SY5Y cells upon Complex II inhibition (Figure 5a). Interestingly, a similar result was observed upon inhibition of mitochondrial ATP synthase by Oligomycin (Figure 5a)

We then investigated the mechanism underlying SERCA2b and PMCA2 down-regulation upon complex II or ATP synthase inhibition. SERCA and PMCA down-regulation could be due to reduced transcription level or increased rate of degradation. By using semi-quantitative RT-PCR, we showed that SERCA2b and PMCA2 transcription level is not altered upon Complex II or ATP synthase inhibition (Figure 5b). We then investigated SERCA2b and PMCA2 degradation. SH-SY5Y Cells were treated with the protein synthesis inhibitor cyclohexemide in the presence or not of Complex II inhibitor (3-NP) or ATP synthase inhibitor (Oligomycin). Kinetic analyses revealed a rapid degradation of both SERCA2b and PMCA2 upon Complex II or ATP synthase (Figure 5c) inhibition. These results showed that Complex II-dependent SERCA and PMCA down-regulation is due to their rapid degradation. To determine whether SERCA2b and PMCA are degraded by the proteasome, we treated the cells with the proteasome inhibitor MG132 for 2 h and then applied cyclohexemide alone or in the presence of 3-NP and Oligomycin for 1 h. As shown in Figure 5d, treatment of the cells with MG132 prevented SERCA2b and PMCA2 degradation upon Complex II or ATP synthase inhibition (Figure 5d).

These data reveal the role of the proteasome-dependent degradation pathway in SERCA2b and PMCA2 down-regulation. The result obtained upon ATP synthase blockade by Oligomycin may reveal that rapid degradation of SERCA2b and PMCA2 is an ATP-dependent mechanism. All over, these data suggests that cytosolic and mitochondrial Ca^{2+} overload upon Complex II deficiency are a consequence of suppressed cytosolic Ca^{2+}

extrusion through the plasma membrane and accumulation in ER by PMCA and SERCA respectively.

As mitochondrial Ca^{2+} overload is a major actor triggering mitochondrial structure alteration and swelling, we then analyzed the mitochondrial structure in the context of Complex II defect. High resolution imaging analyses of mitochondrial structure revealed no clear mitochondrial structure modification in Complex II deficient cells as compared to controls (Supplementary Figure S4a). Accordingly, mitochondrial volume was also not modified upon Complex II mutation or inhibition in both fibroblasts and SH-SY5Y cells (Supplementary Figure S4b). These data are in accordance with the absence of apoptosis in both models and showed also that increased mitochondrial Ca^{2+} content is not associated with increased mitochondrial biogenesis (as estimated by unchanged volume).

It has been demonstrated that elevated Ca^{2+} signals in micro-domains between mitochondria and ER Ca^{2+} release sites immobilize mitochondria close to the ER, thus increasing Ca^{2+} transfer between the organelles (23). Since we showed that Complex II mutation induced on the one hand an increased ER Ca^{2+} leak and on the other hand an elevation of mitochondrial Ca^{2+} load (Figure 4c and Figure 2b and d), we tested whether these modifications are associated with mitochondrial movement inhibition and ER-mitochondria increased contact sites. Indeed, high resolution time-lapse imaging of the mitochondrial network revealed a significant reduction of mitochondrial movements upon Complex II mutation or inhibition in both fibroblasts and SH-SY5Y cells (Figure 6a and Supplementary Table S10). Accordingly, high resolution imaging revealed an increase of the extent of association between ER and mitochondria upon Complex II deficiency (Figure 6b and Supplementary Table S11).

We then investigated the impact of Ca^{2+} deregulation on cellular bioenergetics and mitochondrial dysfunction related to Complex II deficiency.

Measurement of total ATP level on total cell homogenates revealed increased total [ATP] in $\text{SDHA}_{\text{R554W}}$ fibroblasts and in control fibroblasts treated with Atpenin A5 (~ + 15 % vs. control) (Figure 7a and Supplementary Table S12). Similar results were obtained in SH-SY5Y cells upon Complex II inhibition (Figure 7b and Supplementary Table S12). Besides the mitochondrial respiratory chain, glycolysis constitutes a second source of cellular ATP. Since we showed a decrease of $[\text{ATP}]_{\text{mit}}$ (Figure 1d and e), the increased total [ATP] is expected to be due to glycolysis activation. Indeed, glycolysis inhibition with 2-deoxy-D-glucose (2-DG) (a non-metabolizable analog of glucose) leads to a decrease of total [ATP] (Figure 7a and b, and Supplementary Table S12). In agreement with this result,

hyperlactatemia derived from increased glycolysis has been reported in SDHA_{R554W} fibroblasts (14). It has been recently shown that intracellular Ca²⁺ may activate glycolytic ATP synthesis (24). Accordingly, we showed that Ca²⁺ chelation by BAPTA, AM reduced total [ATP] in control and Complex II deficient cells (Figure 7c and Supplementary Table S13). Interestingly, the extent of ATP reduction was larger in Complex II deficient cells as compared to controls (72 % in control, 60 % in SDHA_{R554W} and 65 % in Atpenin A5) (Figure 7c and Supplementary Table S13), suggesting that increased glycolytic ATP production upon Complex II deficiency may have resulted from Ca²⁺ overload as a compensation to decreased mitochondrial ATP loss.

The data presented in Figure 1 showed an overt mitochondrial pathology upon Complex II deficiency. Different laboratories have reported the complex cross-interactions between $\Delta\psi_{mit}$, Ca²⁺ and ROS production (1). It was also shown that mitochondrial depolarization requires and is maintained by the high [Ca²⁺]_{cyt} (25). We thus investigated the role of cytosolic Ca²⁺ overload on $\Delta\psi_{mit}$ loss linked to Complex II deficiency. As shown in Figure 7d, application of BAPTA, AM rescue mitochondrial potential in SDHA_{R554W} cells (Figure 7d and Supplementary Table S14). We assume that mitochondrial potential recovery observed in SDHA_{R554W} is due to reduced mitochondrial Ca²⁺ uptake as a consequence of removal of [Ca²⁺]_{cyt} by BAPTA, AM. Indeed, BAPTA, AM application reduces mitochondrial basal and agonist-evoked [Ca²⁺] (data not shown). In accordance with this result, cell treatment with BAPTA, AM also revealed a significant reduction of [O₂^{•-}] in SDHA_{R554W} cells (Figure 7e and Supplementary Table S15). These findings suggest that Ca²⁺ overload participated to mitochondrial pathology observed in Complex II deficient cells.

We finally addressed the question about the final consequences of mitochondrial pathology upon Complex II deficiency. In accordance with previously reported data (26, 27), we showed that complete Complex II inhibition (1 mM 3NP treatment for 20 h) (Supplementary Figure S1d, right panel) determined cell death (Supplementary Figure S1d, left panel), mitochondrial structure alteration (Supplementary Figure S5a) and reduction of mitochondrial Ca²⁺ load (Supplementary Figure S5b). These processes are known as markers of mitochondrial outer membrane permeabilization and swelling accompanying cell death.

Discussion

By studying fibroblasts isolated from a patient affected by Leigh's syndrome harbouring respiratory chain Complex II (SDHA_{R554W}) mutation (13) and fibroblasts and neuronal derived cells chronically treated with Complex II inhibitors, we reported subcellular Ca²⁺-deregulations occurring prior to cell death and showed that Complex II deficiency induced a deep regulation of Ca²⁺ signalling-dependent bioenergetics and mitochondrial dysfunction which control cellular fate.

Only few studies have been focusing on the study of Complex II inhibition and none has provided a global assessment of subcellular Ca²⁺ signalling prior to cell death. These studies reported that inhibition of Complex II by 3-NP enhances basal and NMDA-induced intracellular [Ca²⁺] in neurons (26, 28, 29), potentially leading to $\Delta\Psi_{mit}$ loss, mitochondrial structure alteration, ROS production and cell death (26, 29, 30).

The parallel and thorough investigation of subcellular Ca²⁺ and bioenergetics alterations upon Complex II mutation or chronic inhibition allowed us to reveal the following pattern (Figure 8): Complex II deficiency is associated with the a proteasome-dependent degradation of the two key Ca²⁺ ATPases, SERCA and PMCA thus leading to increase cytosolic Ca²⁺ signals. Increased [Ca²⁺]_{cyt} and ER Ca²⁺ leak likely caused increased [Ca²⁺]_{mit} through increased ER-mitochondria contact sites and mitochondrial immobilization.

The situation in Complex II deficient cells is particular since a large number of studies have reported reduced Ca²⁺ signals (cytosolic and mitochondrial) in different models of mitochondrial respiratory chain diseases (in MELAS: mitochondrial encephalopathy, lactic acidosis and stroke-like episodes (10), MERRF: myoclonic epilepsy and ragged-red fibres (9), NARP: neurogenic muscle weakness, ataxia and retinitis pigmentosa) (31), and in Complex I mutated fibroblasts (11). To note, our study was conducted in models prior to cell death thus revealing primary Ca²⁺ deregulation events occurring upon Complex II deficiency.

Importantly mitochondrial pathology associated with respiratory chain deficiency can be reverted by counteracting Ca²⁺ signalling deregulation, namely by using BAPTA, AM (this work) or by increasing [Ca²⁺]_{mit} through inhibition of the mitochondrial Na⁺/Ca²⁺ exchanger (9, 32). This leads us to conclude that Ca²⁺ homeostasis deregulation plays a pivotal role in mitochondrial related pathology.

We demonstrated that cytosolic and mitochondrial Ca²⁺ overload linked to Complex II deficiency are likely to be due to rapid degradation of SERCA2b and PMCA2 occurring in a proteasome-dependent manner. This phenomenon is predictably related to the decreased

mitochondrial ATP production, since SERCA2b and PMCA2 degradation was also observed upon ATP synthase inhibition. Complex II-dependent SERCA2b and PMCA2 degradation occurs despite the slight increase of glycolysis-dependent, cytosolic [ATP] pointing out a primary role of mitochondrial ATP in the degradation process. Indeed, mitochondrial ATP is considered the major cellular ATP source. Alternatively, and not exclusively, the proximity between mitochondria and plasma and/or ER membranes could explain the sensitivity of SERCA2b and PMCA2 to mitochondrial ATP production. Accordingly, the existence of ATP micro-domains beneath the plasma membrane and in ER-mitochondria contact sites has been already demonstrated in some cell models (33, 34).

Proteasome-dependent degradation of SERCA2a isoform was reported in a previous work by Ihara et al in 2005 (35). To our knowledge, proteasome-dependent degradation of PMCA has not been reported before. However, ubiquitination of PMCA1 isoform has been detected after preconditioning ischemia in rat cortical neuronal cultures (36). Since polyubiquitylated proteins are the preferred proteasome 26S substrates (37), we postulate that SERCA2b and PMCA2 undergo proteasome-dependent degradation after their ubiquitination. Further analyses are necessary to demonstrate this phenomenon.

It is largely known that ATP/Mg²⁺ regulates the 26S proteasome activity, its assembly and stability (38, 39). However, Geng, Q et al. showed that a subset of 26S proteasome is activated as ATP levels decline (40). In the context of Complex II deficiency, mitochondrial ATP depletion may have favored the activation of a subsets of 26S proteasome leading to SERCA2b and PMCA2 degradation.

Kinetic analyses revealed that increased mitochondrial Ca²⁺ signals occur prior to $\Delta\psi_{mit}$ loss (presumably before mitochondrial ATP decrease) suggesting a potential additional mechanism, independently from SERCA2b and PMCA2 degradation, involved in increased mitochondrial [Ca²⁺] upon Complex II inhibition (4 h-6 h). Since 99.9 % of the total matrix Ca²⁺ content is in bound form (41), we cannot exclude a role for an increased mitochondrial retention capacity in the observed mitochondrial Ca²⁺ overload (e. g. Ca²⁺ binding to cardiolipin, anionic phospholipids, the carboxy-anion-containing metabolites of the Krebs cycle (citrate, oxaloacetate) and inorganic phosphate (41)).

Increased total ATP production has been recently reported in MELAS syndrome linked to Complex I ND5 gene mutation (42). In this study, glycolytic ATP has been shown to be consumed by mitochondria to maintain $\Delta\psi_{mit}$. In addition, Ca²⁺-dependent activation of anaerobic glycolysis and increased cytosolic ATP have been recently described during apoptotic cell death (24). Since our study was conducted prior to cell death, increased

glycolysis-dependent [ATP] may be a compensatory mechanism to the decreased oxidative phosphorylation-dependent ATP production. This phenomenon is Ca^{2+} -dependent since we showed that Ca^{2+} chelation by BAPTA, AM reversed glycolytic-dependent ATP production.

Thus, the increase of intracellular Ca^{2+} signals may be considered as a first attempt to delay cellular pathology through the activation of glycolytic-dependent ATP production.

Our study revealed a double hint of Ca^{2+} signalling deregulation in Complex II deficient cells since besides increasing glycolytic ATP production, Ca^{2+} overload favored mitochondrial pathology. Thus, depending on their energetic needs, cells with Complex II defect may thus undergo a progressive mitochondrial dysfunction, characterized by $\Delta\psi_{\text{mit}}$ loss, Ca^{2+} overload, and increased ROS, eventually leading to cell death (Supplementary Figure S5). As a matter of fact, neuronal loss was reported in the brain of the patient harboring $\text{SDHA}_{\text{R554W}}$ mutation (43).

Materials and methods

Chemicals. Culture material was obtained from Invitrogen, coelenterazine, and fluorescent dyes from Molecular Probes (Invitrogen, SARL), and Atpenin A5 from Coger (eMarketLabo.com). All the other reagents and chemicals were from Sigma-Aldrich (Sigma-Aldrich, SARL).

Cell culture. Fibroblasts were grown as already described (19). Human SH-SY5Y neuroblastoma cells (CRL-2266: ATCC) were cultured following manufacturer's instructions.

Aequorin measurements. To bypass low transfection efficiency of fibroblasts and SH-SY5Y cells, we used the previously described adenoviral system expressing cytosolic-(AdCMVcytAEQ), mitochondrial-(AdCMVmitAEQmut and AdCMVmitAEQwt), and ER-(AdCMVerAEQ) targeted aequorin probes (44-46). For infection, approximately 20000 cells (fibroblasts) and 150000 cells (SH-SY5Y) were spotted on 13-mm coverslips, and placed 24 h later in contact with the appropriate virus (10^5 infectious particles/ml). Aequorin measurements were performed 48 h post infection. Specific targeting of adenoviral aequorin probes to desired organelles was verified by immunohistochemistry (Supplementary Figure S6).

MitAEQ and cytAEQ were reconstituted with 5 μ M coelenterazine for 2 h in Krebs-Ringer modified buffer (KRB: 125 mM NaCl, 5 mM KCl, 1 mM Na_3PO_4 , 1 mM MgSO_4 , 5.5 mM glucose, and 20 mM HEPES, pH 7.4) supplemented with 1 mM CaCl_2 (KRB/ CaCl_2) at 37 °C. Cytosolic and mitochondrial signals were obtained upon application of 100 μ M Histamine (fibroblasts) or 500 μ M Carbachol (SH-SY5Y).

Capacitative Ca^{2+} entry analyses were performed by using cytosolic-(AdCMVcytAEQ) aequorin probe. Cells transferred to the luminometer were treated as specified in the legend of the figure.

For reconstitution with high efficiency of the erAEQ, the luminal [Ca^{2+}] of this compartment was first reduced. This was achieved by incubating the cells for 1 h at 4 °C in KRB supplemented with 5 μ M n-coelenterazine, 1 μ M Ca^{2+} ionophore ionomycin and 600 μ M EGTA. After this incubation, cells were extensively washed with KRB supplemented with 2 % bovine serum albumin (BSA) before the luminescence measurement was initiated. The ER was refilled by exposing the cells to extracellular 1 mM CaCl_2 . After reaching the steady state value, agonist evoked Ca^{2+} release was initiated by application of agonists. The SERCA blocker, TBuBHQ (2, 5 -Di (tert-butyl) - 1, 4 - benzohydroquinone) was used to initiate the release of stored Ca^{2+} and thus to analyse ER Ca^{2+} leak. All aequorin measurements were

carried out in a purpose built luminometer. The experiments were terminated by lysis of the cells with 100 μM digitonin in a hypotonic Ca^{2+} -rich solution (10 mM CaCl_2 in H_2O), thus discharging the remaining aequorin pool. The light signal was collected and calibrated into $[\text{Ca}^{2+}]$ values, as previously described (22). Based on the experimental traces, the maximum rates of ER Ca^{2+} uptake were measured from the first derivative of the ascending refilling phase obtained after CaCl_2 addition, and the maximum rates of ER Ca^{2+} leak were measured from the first derivative of the curve upon addition of TBuBHQ using Origin 5 software. Fitting of the curve was performed using Microsoft Excel software.

$[\text{Ca}^{2+}]_{\text{mit}}$ in permeabilized cells. After infection with AdCMVmitAEQ and AEQ reconstitution, plasma membrane was permeabilized for 1 min by perfusing with 25 μM digitonin. After permeabilization, cells were perfused with an intracellular mimicking buffer (IB: 120 mM KCl, 10 mM NaCl, 2 mM KH_2PO_4 , 1 mM MgCl_2 , 10 mM Hepes, 1 mM succinic acid, 1 mM pyruvic acid, 50 μM EGTA, and 2 mM of ATP/ MgCl_2 , pH 7.4 at 37 $^\circ\text{C}$). This experimental setting largely renders mitochondrial Ca^{2+} concentration independent of contacts sites with the ER and was used to assess the activity of Ca^{2+} uptake and extrusion mechanisms.

After a brief wash, mitochondrial Ca^{2+} uptake was initiated by perfusing IB buffered free $[\text{Ca}^{2+}]$ (1.5). Mitochondrial Ca^{2+} efflux was initiated by application of the mitochondrial uniporter inhibitor ruthenium red (RuR) (10 μM). Cyclosporin A (CSA) (0.5 μM) was used to inhibit mitochondrial permeability transition pore (PTP).

ATP measurements. Mitochondrial [ATP] was measured after transient transfection of mitochondrial targeted luciferase probe (mit-LUC) as already described (9). Briefly, cell luminescence was measured in the same luminometer used for aequorin measurements. Cells were perfused with KRB, supplemented with 1 mM CaCl_2 and then shifted to the same buffer supplemented with 20 μM luciferin. At the end of each experiment, cells were permeabilized with digitonin (25 μM) and placed in IB) supplemented with, 5 mM of ATP/ MgCl_2 and 20 μM luciferin. Mitochondrial basal ATP level was normalized to the maximum luciferase signal obtained after cell permeabilization with digitonin and considered as 100 %. For total ATP level we used ATP Bioluminescence Assay kit CL II (Roche).

Measurements of cytosolic and mitochondrial basal $[\text{Ca}^{2+}]$ concentrations. Cells spotted on 24-mm coverslips were loaded with 5 μM Fluo-4, AM (cytosolic Ca^{2+} probe) or 1 μM X-rhod-1, AM (mitochondrial Ca^{2+} probe) prepared in a KRB/1 mM CaCl_2 at 37 $^\circ\text{C}$ for 30 min. After a brief washout, time lapse images were acquired on a Zeiss LSM 510 confocal

microscope (Carl Zeiss). We calibrated Fluo4, AM and X-Rhod-1, AM probes as recently described by our group (22) and provided absolute basal Ca^{2+} values in the cytosol and the mitochondria. Following a control period (providing the basal fluorescent intensity, F), F_{\max} was obtained upon application of ionomycin/ Ca^{2+} solution (ionomycin: 10 μM and Ca^{2+} : 50 mM). Then, the F_{\min} value was obtained upon addition of 10 mM EGTA solution in the same bath. We used the equation provided by the manufacturer ($[\text{Ca}^{2+}]_{\text{free}} = K_d * ((F - F_{\min}) / (F_{\max} - F))$) and the K_d value of 700 nM for X-Rhod-1, AM and of 345 nM for Fluo4, AM.

Measurements of mitochondrial superoxide concentration. MitoSOX Red is a novel fluorogenic dye recently developed and validated (47) for highly selective detection of superoxide in the mitochondria of living cells. Cells spotted on 24-mm coverslips were loaded with 5 μM MitoSOX red prepared in a KRB/1 mM CaCl_2 at 37 °C for 30 min. After a brief washout, Z-stack images were acquired on a Zeiss LSM 510 confocal microscope (Carl Zeiss). Dye intensity was quantified on maximal projection of Z-stack images after thresholding, using the Zeiss LSM and ImageJ softwares. We presented data as mean fluorescence intensity of oxidized MitoSOX. We assume that MitoSOX probe give a semi quantitative detection and not an absolute estimation of mitochondrial superoxide value. Importantly, as control we used the ROS scavenger PDCT to show the specificity of this probe.

Imaging analyzes. For the measurement of mitochondrial movements or mitochondrial potential ($\Delta\psi_{\text{mit}}$), images were acquired on a Zeiss LSM 510 confocal microscope after loading the cells with 10 nM Mitotracker red (movement analysis) or 20 nM tetramethyl rhodamine methyl ester (TMRM) ($\Delta\psi_m$ analysis) in KRB/1 mM CaCl_2 at 37°C for 30 min. For mitochondria movement analysis, time series images were taken with a time interval of 5 s between each image. Images were 2D-deconvolved, median filtered, thresholded and clipped to 8 bit binary images using Metamorph (Universal Imaging) software. Using the stack-T-functions/Delta-F-down plugin of the WCIF ImageJ software (<http://www.uhnres.utoronto.ca/facilities/wcif/>), pixels in each frame were subtracted from the next frame. The resulting images were quantified by measuring the total area of object on the binary and ΔF images by the Integrated Morphometry Analysis function of the Metamorph software. Data were normalized as the ratio of ΔF area values over the total area of the original binary images for each cell. This parameter is referred to as the mitochondrial movement index (MI) (22). Binarization and normalization were applied to avoid artefacts eventually arising from changes of intensity and focal plane.

To obtain normalized TMRM fluorescence signal, time lapse images were acquired on a Zeiss LSM 510 confocal microscope. Images were acquired before and after application of 10 μM mitochondrial uncoupler FCCP. To demonstrate specific TMRM binding, measurements were routinely corrected for residual TMRM fluorescence after full $\Delta\psi_{\text{mit}}$ collapse with the mitochondrial uncoupler FCCP (48). Basal TMRM signal was normalized to the remaining signal obtained upon FCCP application and presented as f/f_0 where f is the mean of basal TMRM intensity along 10 s in the plateau phase and f_0 the mean of TMRM intensity along the baseline after FCCP application.

For analyzes of ER-mitochondria contact sites, cells were transfected with erGFP and loaded with Mitotracker Deep Red. The spectral properties of these two fluorochromes allow specific identification of the two compartments and quantification of contact sites. 16-bit images were acquired with a pixel size equal or lower to the maximal resolution of the 63X-objective to allow optimal detection of colocalized pixels on the stage of a Leica SP5 confocal microscope. ER and mitochondria colocalization was calculated as the number of voxels (volume pixels) occupied by both signals (i.e. erGFP and Mitotracker Deep Red) over all voxels occupied by the mitochondria (Mitotracker Deep Red signal) in thresholded images using Imaris software.

Protein preparation and western-blot analyses. Plasma membrane and microsomal fractions were isolated as already described (22, 49). SDS-PAGE was then performed. The signal was revealed using ECL Plus Western blot detection reagent (Amersham Biosciences). For the experiments shown in figure 5 c and d, membrane fraction obtained as already described (22) was used to reveal both SERCA and PMCA. Protein synthesis was inhibited using 100 μM cyclohexemide (CHX) alone or in the presence of 300 μM 3-NP or 5 μM Oligomycin for the indicated time points. Proteasome-dependent degradation of SERCA2b and PMCA2 was assessed using proteasome inhibitor MG132. After 2 h pre-incubation of SH-SY5Y cells with or without MG132 (5 μM), cells were treated for 1 h with 100 μM cyclohexemide in the presence or not of 300 μM 3-NP or 5 μM Oligomycin. Loading control was assessed using α tubulin, GRP94 as a marker of a resident endoplasmic reticulum protein and cadherin as a marker of a resident plasma membrane protein. Similar result was obtained using these loading controls. Only the result of α tubulin is shown.

RNA extraction and RT-PCR analysis. Total RNA was extracted using RNeasy Mini kit (Qiagen). One μg of total RNA was used for reverse transcription using High-Capacity cDNA Archive Kit (Applied Biosystems) with random hexamer primers according to the

manufacturer's protocol. The final reaction volume was 25 μ l. The reaction tubes were incubated at 25°C for 10 min, 120 min at 37°C and 5 min at 85 °C. The primers for polymerase chain reaction (PCR) for PMCA2 transcript were forward: TCCCGACCAGCAGACTCAAGTT, reverse: CGAGTTCTGCTTGAGCGCGG (fragment size: 350 bp). For SERCA 2b transcript, the following primers were used: forward: TTCCTACAGTGTAAGAGGACAACC, reverse: AGACCAGAACATATCGCTAAAGTT (fragment size: 514 bp). PMCA and SERCA2b transcript levels were normalized to GAPDH transcript level amplified using forward: CTCATTGACCTCAACTACATGGT, reverse: CTCAGTGTAGCCCAGGATGCCCTT (fragment size: 727 bp). PCR was performed using 0.5 μ l of the reverse transcription mixture in a final volume of 50 μ l containing: 1X Green GoTaq buffer, primers (10 μ M each) and Gren Go Taq Hot start polymerase (2.5 U) and dNTP (10 mM each). PCR amplification cycles were run using a thermal cycler (Perkin-Elmer) as following: denaturation at 95 °C, 5 min; annealing at 60 °C, 1 min; extension at 72 °C, 1 min, and heating at 72 °C, 10 min. For semi-quantitative PCR, three different amplification cycles were used see figure legend. Relative signal intensities were quantified using NIH Image J software and are shown in graphs.

Statistical analyses. Results are reported from at least three different experiments. Statistical analyses were done using ANOVA. Bonferroni *Post hoc* analysis were subsequently performed on ANOVA results to determine significance. Bonferroni t test was calculated versus respective control (Supplementary Tables S1-11) and graphs in Figure 5, or all pairwise (Supplementary Tables S12-15).

References

1. Brookes PS, Yoon Y, Robotham JL, Anders MW, Sheu SS. Calcium, ATP, and ROS: a mitochondrial love-hate triangle. *Am J Physiol Cell Physiol* 2004 Oct; **287** (4): C817-833.
2. Hajnoczky G, Hager R, Thomas AP. Mitochondria suppress local feedback activation of inositol 1,4, 5-trisphosphate receptors by Ca²⁺. *J Biol Chem* 1999 May 14; **274** (20): 14157-14162.
3. McCormack JG, Halestrap AP, Denton RM. Role of calcium ions in regulation of mammalian intramitochondrial metabolism. *Physiol Rev* 1990 Apr; **70** (2): 391-425.
4. Benit P, Slama A, Cartault F, Giurgea I, Chretien D, Lebon S, *et al.* Mutant NDUFS3 subunit of mitochondrial complex I causes Leigh syndrome. *J Med Genet* 2004 Jan; **41** (1): 14-17.
5. Lebon S, Minai L, Chretien D, Corcos J, Serre V, Kadhom N, *et al.* A novel mutation of the NDUFS7 gene leads to activation of a cryptic exon and impaired assembly of mitochondrial complex I in a patient with Leigh syndrome. *Mol Genet Metab* 2007 Sep-Oct; **92** (1-2): 104-108.
6. Pagnamenta AT, Hargreaves IP, Duncan AJ, Taanman JW, Heales SJ, Land JM, *et al.* Phenotypic variability of mitochondrial disease caused by a nuclear mutation in complex II. *Mol Genet Metab* 2006 Nov; **89** (3): 214-221.
7. Zhu Z, Yao J, Johns T, Fu K, De Bie I, Macmillan C, *et al.* SURF1, encoding a factor involved in the biogenesis of cytochrome c oxidase, is mutated in Leigh syndrome. *Nat Genet* 1998 Dec; **20** (4): 337-343.
8. Schon EA, Santra S, Pallotti F, Girvin ME. Pathogenesis of primary defects in mitochondrial ATP synthesis. *Semin Cell Dev Biol* 2001 Dec; **12** (6): 441-448.
9. Brini M, Pinton P, King MP, Davidson M, Schon EA, Rizzuto R. A calcium signaling defect in the pathogenesis of a mitochondrial DNA inherited oxidative phosphorylation deficiency. *Nat Med* 1999; **5** (8): 951-954.
10. Moudy AM, Handran SD, Goldberg MP, Ruffin N, Karl I, Kranz-Eble P, *et al.* Abnormal calcium homeostasis and mitochondrial polarization in a human encephalomyopathy. *Proc Natl Acad Sci U S A* 1995 Jan 31; **92** (3): 729-733.
11. Visch HJ, Koopman WJ, Leusink A, van Emst-de Vries SE, van den Heuvel LW, Willems PH, *et al.* Decreased agonist-stimulated mitochondrial ATP production caused by a pathological reduction in endoplasmic reticulum calcium content in human complex I deficiency. *Biochim Biophys Acta* 2006 Jan; **1762** (1): 115-123.
12. Ackrell BA. Progress in understanding structure-function relationships in respiratory chain complex II. *FEBS Lett* 2000 Jan 21; **466** (1): 1-5.

13. Bourgeron T, Rustin P, Chretien D, Birch-Machin M, Bourgeois M, Viegas-Pequignot E, *et al.* Mutation of a nuclear succinate dehydrogenase gene results in mitochondrial respiratory chain deficiency. *Nat Genet* 1995 Oct; **11** (2): 144-149.
14. Birch-Machin MA, Marsac C, Ponsot G, Parfait B, Taylor RW, Rustin P, *et al.* Biochemical investigations and immunoblot analyses of two unrelated patients with an isolated deficiency in complex II of the mitochondrial respiratory chain. *Biochem Biophys Res Commun* 1996 Mar 7; **220** (1): 57-62.
15. Huang LS, Sun G, Cobessi D, Wang AC, Shen JT, Tung EY, *et al.* 3-nitropropionic acid is a suicide inhibitor of mitochondrial respiration that, upon oxidation by complex II, forms a covalent adduct with a catalytic base arginine in the active site of the enzyme. *J Biol Chem* 2006 Mar 3; **281** (9): 5965-5972.
16. Miyadera H, Shiomi K, Ui H, Yamaguchi Y, Masuma R, Tomoda H, *et al.* Atpenins, potent and specific inhibitors of mitochondrial complex II (succinate-ubiquinone oxidoreductase). *Proc Natl Acad Sci U S A* 2003 Jan 21; **100** (2): 473-477.
17. Echtay KS, Roussel D, St-Pierre J, Jekabsons MB, Cadenas S, Stuart JA, *et al.* Superoxide activates mitochondrial uncoupling proteins. *Nature* 2002 Jan 3; **415** (6867): 96-99.
18. Iuso A, Scacco S, Piccoli C, Bellomo F, Petruzzella V, Trentadue R, *et al.* Dysfunctions of cellular oxidative metabolism in patients with mutations in the NDUFS1 and NDUFS4 genes of complex I. *J Biol Chem* 2006 Apr 14; **281** (15): 10374-10380.
19. Geromel V, Kadhom N, Cebalos-Picot I, Ouari O, Polidori A, Munnich A, *et al.* Superoxide-induced massive apoptosis in cultured skin fibroblasts harboring the neurogenic ataxia retinitis pigmentosa (NARP) mutation in the ATPase-6 gene of the mitochondrial DNA. *Hum Mol Genet* 2001 May 15; **10** (11): 1221-1228.
20. Jouaville LS, Pinton P, Bastianutto C, Rutter GA, Rizzuto R. Regulation of mitochondrial ATP synthesis by calcium: evidence for a long-term metabolic priming. *Proc Natl Acad Sci U S A* 1999 Nov 23; **96** (24): 13807-13812.
21. Murgia M, Giorgi C, Pinton P, Rizzuto R. Controlling metabolism and cell death: At the heart of mitochondrial calcium signalling. *J Mol Cell Cardiol* 2009 Mar 12.
22. Chami M, Oules B, Szabadkai G, Tacine R, Rizzuto R, Paterlini-Brechot P. Role of SERCA1 truncated isoform in the proapoptotic calcium transfer from ER to mitochondria during ER stress. *Mol Cell* 2008 Dec 5; **32** (5): 641-651.
23. Yi M, Weaver D, Hajnoczky G. Control of mitochondrial motility and distribution by the calcium signal: a homeostatic circuit. *J Cell Biol* 2004 Nov 22; **167** (4): 661-672.
24. Zamaraeva MV, Sabirov RZ, Manabe K, Okada Y. Ca(2+)-dependent glycolysis activation mediates apoptotic ATP elevation in HeLa cells. *Biochem Biophys Res Commun* 2007 Nov 23; **363** (3): 687-693.

25. Abramov AY, Duchen MR. Mechanisms underlying the loss of mitochondrial membrane potential in glutamate excitotoxicity. *Biochim Biophys Acta* 2008 Jul-Aug; **1777** (7-8): 953-964.
26. Liot G, Bossy B, Lubitz S, Kushnareva Y, Sejbuk N, Bossy-Wetzel E. Complex II inhibition by 3-NP causes mitochondrial fragmentation and neuronal cell death via an NMDA- and ROS-dependent pathway. *Cell Death Differ* 2009 Jun; **16** (6): 899-909.
27. Lim D, Fedrizzi L, Tartari M, Zuccato C, Cattaneo E, Brini M, *et al.* Calcium homeostasis and mitochondrial dysfunction in striatal neurons of Huntington disease. *J Biol Chem* 2008 Feb 29; **283** (9): 5780-5789.
28. Calabresi P, Gubellini P, Picconi B, Centonze D, Pisani A, Bonsi P, *et al.* Inhibition of mitochondrial complex II induces a long-term potentiation of NMDA-mediated synaptic excitation in the striatum requiring endogenous dopamine. *J Neurosci* 2001 Jul 15; **21** (14): 5110-5120.
29. Nasr P, Gursahani HI, Pang Z, Bondada V, Lee J, Hadley RW, *et al.* Influence of cytosolic and mitochondrial Ca²⁺, ATP, mitochondrial membrane potential, and calpain activity on the mechanism of neuron death induced by 3-nitropropionic acid. *Neurochem Int* 2003 Jul; **43** (2): 89-99.
30. Rosenstock TR, Carvalho AC, Jurkiewicz A, Frussa-Filho R, Smaili SS. Mitochondrial calcium, oxidative stress and apoptosis in a neurodegenerative disease model induced by 3-nitropropionic acid. *J Neurochem* 2004 Mar; **88** (5): 1220-1228.
31. Szczepanowska J, Zablocki K, Duszynski J. Influence of a mitochondrial genetic defect on capacitative calcium entry and mitochondrial organization in the osteosarcoma cells. *FEBS Lett* 2004 Dec 17; **578** (3): 316-322.
32. Visch HJ, Rutter GA, Koopman WJ, Koenderink JB, Verkaart S, de Groot T, *et al.* Inhibition of mitochondrial Na⁺-Ca²⁺ exchange restores agonist-induced ATP production and Ca²⁺ handling in human complex I deficiency. *J Biol Chem* 2004 Sep 24; **279** (39): 40328-40336.
33. Kaasik A, Veksler V, Boehm E, Novotova M, Minajeva A, Ventura-Clapier R. Energetic crosstalk between organelles: architectural integration of energy production and utilization. *Circ Res* 2001 Jul 20; **89** (2): 153-159.
34. Kennedy HJ, Pouli AE, Ainscow EK, Jouaville LS, Rizzuto R, Rutter GA. Glucose generates sub-plasma membrane ATP microdomains in single islet beta-cells. Potential role for strategically located mitochondria. *J Biol Chem* 1999 May 7; **274** (19): 13281-13291.
35. Ihara Y, Kageyama K, Kondo T. Overexpression of calreticulin sensitizes SERCA2a to oxidative stress. *Biochem Biophys Res Commun* 2005 Apr 22; **329** (4): 1343-1349.
36. Meller R, Thompson SJ, Lusardi TA, Ordonez AN, Ashley MD, Jessick V, *et al.* Ubiquitin proteasome-mediated synaptic reorganization: a novel mechanism underlying rapid ischemic tolerance. *J Neurosci* 2008 Jan 2; **28** (1): 50-59.

37. Depraetere V. Getting activated with poly-ubiquitination. *Nat Cell Biol* 2001 Aug; **3** (8): E181.
38. Babbitt SE, Kiss A, Deffenbaugh AE, Chang YH, Bailly E, Erdjument-Bromage H, *et al.* ATP hydrolysis-dependent disassembly of the 26S proteasome is part of the catalytic cycle. *Cell* 2005 May 20; **121** (4): 553-565.
39. Liu CW, Li X, Thompson D, Wooding K, Chang TL, Tang Z, *et al.* ATP binding and ATP hydrolysis play distinct roles in the function of 26S proteasome. *Mol Cell* 2006 Oct 6; **24** (1): 39-50.
40. Geng Q, Romero J, Saini V, Baker TA, Picken MM, Gamelli RL, *et al.* A subset of 26S proteasomes is activated at critically low ATP concentrations and contributes to myocardial injury during cold ischemia. *Biochem Biophys Res Commun* 2009 Dec 25; **390** (4): 1136-1141.
41. Spat A, Szanda G, Csordas G, Hajnoczky G. High- and low-calcium-dependent mechanisms of mitochondrial calcium signalling. *Cell Calcium* 2008 Jul; **44** (1): 51-63.
42. McKenzie M, Liolitsa D, Akinshina N, Campanella M, Sisodiya S, Hargreaves I, *et al.* Mitochondrial ND5 gene variation associated with encephalomyopathy and mitochondrial ATP consumption. *J Biol Chem* 2007 Dec 21; **282** (51): 36845-36852.
43. Burgeois M, Goutieres F, Chretien D, Rustin P, Munnich A, Aicardi J. Deficiency in complex II of the respiratory chain, presenting as a leukodystrophy in two sisters with Leigh syndrome. *Brain Dev* 1992 Nov; **14** (6): 404-408.
44. Ainscow EK, Rutter GA. Mitochondrial priming modifies Ca²⁺ oscillations and insulin secretion in pancreatic islets. *Biochem J* 2001 Jan 15; **353** (Pt 2): 175-180.
45. Mitchell KJ, Pinton P, Varadi A, Tacchetti C, Ainscow EK, Pozzan T, *et al.* Dense core secretory vesicles revealed as a dynamic Ca²⁺ store in neuroendocrine cells with a vesicle-associated membrane protein aequorin chimera. *J Cell Biol* 2001 Oct 1; **155** (1): 41-51.
46. Mitchell KJ, Tsuboi T, Rutter GA. Role for plasma membrane-related Ca²⁺-ATPase-1 (ATP2C1) in pancreatic beta-cell Ca²⁺ homeostasis revealed by RNA silencing. *Diabetes* 2004 Feb; **53** (2): 393-400.
47. Robinson KM, Janes MS, Pehar M, Monette JS, Ross MF, Hagen TM, *et al.* Selective fluorescent imaging of superoxide in vivo using ethidium-based probes. *Proc Natl Acad Sci U S A* 2006 Oct 10; **103** (41): 15038-15043.
48. Duchen MR, Surin A, Jacobson J. Imaging mitochondrial function in intact cells. *Methods Enzymol* 2003; **361**: 353-389.

49. Chami M, Ferrari D, Nicotera P, Paterlini-Brechot P, Rizzuto R. Caspase-dependent alterations of Ca²⁺ signaling in the induction of apoptosis by hepatitis B virus X protein. *J Biol Chem* 2003 Aug 22; **278** (34): 31745-31755.

ACKNOWLEDGEMENTS

High resolution imaging analyses were performed in Pasteur institute (PFID), Paris, France. Fluorescence imagery analyses were performed in the imaging core facility of Necker-Enfants Malades, Paris V University, France. We thank the vector core of the university Hospital of Nantes supported by the association Française contre les myopathies (AFM) for producing the Adenovirus vectors.

This work was supported by grants from INSERM (Institut National de Santé et Recherche Médicale), AFM (11456 and 13291) and la Fondation pour la Recherche Médicale (FRM) (DEQ20071210550). C. Caspersen was supported by “region Ile de France” postdoctoral fellowship. M. Chami was supported by an INSERM young researcher contract and by the Italian Institute of Technology funds. E. MBaya was supported by a doctoral fellowship from Congo Ministry. We gratefully acknowledge the Ecole de l’INSERM for supporting the MD-PhD curriculum of B. Oulès. GAR was supported by grants from the Wellcome trust (081958/Z/07/Z), MRC (90401641), NIH (DK071962-01) and EU (FP6 “SAVEBETA”). M.P. is supported by Muscular Dystrophy Association and Kennedy Disease Association Grants.

We declare that we do not have competing financial interests.

Figure 1 Mitochondrial function is altered upon Complex II defect. (a, b) $\Delta\Psi_{mit}$, as assessed by TMRM probe in SDHA_{R554W} mutated fibroblasts, and in control fibroblasts (a) and SH-SY5Y cells (b) left untreated (Control) or treated with 300 μ M 3-NP or 100 nM Atpenin A5 for 20 h. Basal TMRM intensity was normalized to the fluorescence drop ($\Delta\Psi_{mit}$ collapse) upon 10 μ M FCCP application. Representative traces show normalized f/f_0 TMRM intensity, where f is the basal TMRM intensity, and f_0 the TMRM intensity after FCCP application. Graphs show normalized TMRM (f/f_0) intensity in % versus control considered as 100 %. Images are representative of TMRM loading in mutated fibroblasts and controls left untreated or treated as detailed before. The mean of normalized TMRM signal \pm SEM, normalized TMRM signal (%) and the number of experiments are represented in Supplementary Table S2. (c) Superoxide content as determined with MitoSOX dye in SDHA_{R554W} fibroblasts, and in control fibroblasts left untreated (Control) or treated as in (a). Representative images of MitoSOX loading are shown. The mean of MitoSOX intensity \pm SEM and the number of experiments are represented in Supplementary Table S3. (d, e) Mitochondrial basal ATP level normalized to the maximum luciferase signal in SDHA_{R554W} and control fibroblasts (d) and in SH-SY5Y cells left untreated (Control) or treated as in (a) (e). Data are expressed as percentage of luciferase light output (CPS: counts per second) with respect to the value obtained after cell permeabilization in the presence of maximal [ATP] (see experimental procedures for details). Representative traces of normalized luciferase signal (% CPS) are shown in the insets. The mean of basal ATP level \pm SEM and the number of experiments are represented in Supplementary Table S4. (a-e) Data are representative of three independent experiments. (*) $P \geq 0.001$, (**) $P < 0.001$ vs Control.

Figure 2 Complex II defect leads to cytosolic and mitochondrial Ca^{2+} signalling deregulation. (a, b) Basal cytosolic [Ca^{2+}] (calibrated Fluo-4, AM intensity, see experimental procedures for details) (a) and basal mitochondrial [Ca^{2+}] (calibrated X-Rhod-1, AM intensity, see experimental procedures for details) (b) in SDHA_{R554W} mutated fibroblasts and in control fibroblasts left untreated (Control) or treated as in Figure 1a. Representative images for Fluo-4, AM and X-Rhod-1, AM loading are shown. The mean value \pm SEM and the number of experiments are indicated in Supplementary Tables S5 and S6. (c, d) Representative curves of agonist-evoked cytosolic Ca^{2+} signal ($[Ca^{2+}]_{cyt}$) (c) and mitochondrial Ca^{2+} signal ($[Ca^{2+}]_{mit}$) (d) in control and SDHA_{R554W} fibroblasts (left panel) and in SH-SY5Y cells (right panel) left untreated (Control) or treated as in Figure 1a. The mean values \pm SEM and the number of experiments are indicated in Supplementary Tables S7 and

S8. **(a-d)** Data are representative of three independent experiments. (*) $P \geq 0.001$, (**) $P < 0.001$ vs Control.

Figure 3 Mitochondrial Ca^{2+} overload occurs early upon complex II deficiency. **(a)** Agonist-evoked mitochondrial Ca^{2+} signal ($[\text{Ca}^{2+}]_{\text{mit}}$) in control fibroblasts and SH-SY5Y cells untreated (Control) or treated with 300 μM 3-NP or 100 nM Atpenin A5 for 2, 4 or 6 h. The mean values \pm SEM and the number of experiments are indicated in Supplementary Table S8. **(b)** $\Delta\psi_{\text{mit}}$, as performed in Figure 1a, and b in control fibroblasts and SH-SY5Y cells untreated (Control) or treated as in (a). Graphs show normalized TMRM intensity (f/f_0). The mean f/f_0 values \pm SEM and the number of experiments are represented in Supplementary Table S2. Data are representative of three independent experiments. (*) $P \geq 0.001$, (**) $P < 0.001$ vs Control.

Figure 4 Increased Intracellular Ca^{2+} signals upon complex II deficiency is associated with deregulated ER Ca^{2+} homeostasis without a modification of calcium entry through plasma membrane. **(a)** Representative curves of ER Ca^{2+} concentration ($[\text{Ca}^{2+}]_{\text{ER}}$) in control and SDHA_{R554W} fibroblasts. Graph: mean \pm SEM. The mean values \pm SEM and the number of experiments are indicated in Supplementary Table S9. **(b)** Dependence on $[\text{Ca}^{2+}]$ of the ER Ca^{2+} uptake rate analysed upon application of CaCl_2 solution (see experimental procedures for details). **(c)** Dependence on $[\text{Ca}^{2+}]$ of the ER Ca^{2+} leak rate analysed upon application of the SERCA inhibitor TBuBHQ (see experimental procedures for details). **(d)** Capacitative Ca^{2+} influx analysis in control and SDHA_{R554W} fibroblasts challenged first with 100 μM histamine in 1 mM EGTA to empty intracellular Ca^{2+} pools and then with 100 μM histamine in 1 mM CaCl_2 to activate Ca^{2+} entry. **(a-d)** Data are representative of three independent experiments. (**) $P < 0.001$ vs Control.

Figure 5 Complex II deficiency is associated with down-regulation of SERCA2b and PMCA expression. **(a)** Western blot analyses of microsomal fraction (SERCA2b and GRP94) and of plasma membrane fraction (PMCA, and transferrin (TFN)) of control and SDHA_{R554W} fibroblasts and SH-SY5Y cells left untreated (Control) or treated with 300 μM 3-NP, 100 nM Atpenin A5 or 5 μM Oligomycin for 20 h. Quantification of SERCA2b protein level was normalized to GRP94 signal and PMCA to TFN signal and is represented in arbitrary units (A.U.). **(b)** SERCA and PMCA expression down-regulation in complex II

deficient cells is not linked to reduced mRNA levels. Semi-quantitative RT-PCR analysis of SH-SY5Y cells left untreated (Control) or treated as in (a). The blots show the results of different cycles of the PCR of SERCA2b (24, 26 and 28 cycles), PMCA2 (32, 34 and 36 cycles) and GAPDH used as control (22, 24, 26 cycles). Quantification of three independent experiments is shown in graphs as mean \pm SEM., ns non-significant vs Control. Representative blots are shown. (c) Rapid degradation of SERCA 2b and PMCA2 upon complex II inhibition by 3-NP (300 μ M) or ATP synthase inhibition by Oligomycin (5 μ M). SH-SY5Y cells were treated with 100 μ M cycloheximide (CHX) alone or in the presence of 3-NP or Oligomycin for the indicated time points. α -Tubulin was used as loading control. Quantification of three independent experiments is shown in graphs as mean \pm SEM., ns non-significant, (*) $P \geq 0.01$ vs untreated cells (Control) considered as 1. Representative blots are shown. (d) Effect of proteasome inhibitor MG132 on SERCA2b and PMCA2 expression. After 2 h pre-incubation of SH-SY5Y cells with or without MG132 (5 μ M), cells were treated for 1 h with 100 μ M cycloheximide in the presence or not of 300 μ M 3-NP or 5 μ M Oligomycin. α -Tubulin was used as loading control.

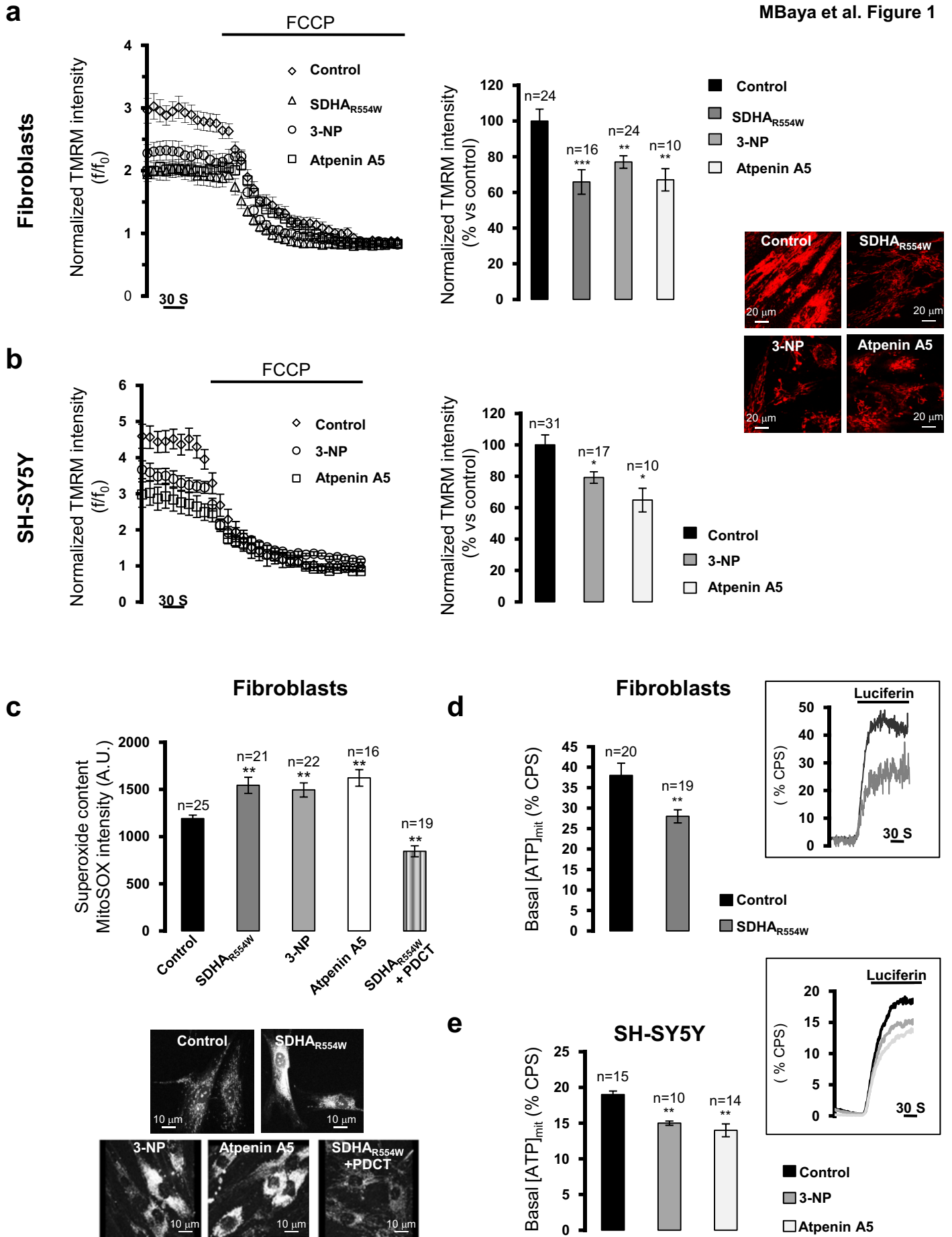
Figure 6 Mitochondrial motility and ER-mitochondria contact sites are modified upon complex II defect. (a) Mitochondrial movement index (MI) was analyzed in the same conditions as in Figure 1a and 1b by using Mitotracker red dye. Images converted to binary files were sequentially subtracted to generate ΔF . MI corresponds to the ratio of ΔF on total mitochondrial area. Data are presented as MI vs Control considered as 1. MI \pm SEM are shown in Supplementary Table S10. (b) ER-mitochondria contact sites were analyzed in cells transfected with erGFP and loaded with MitoTracker Deep Red in the same conditions as in (a). Representative images of ER (erGFP, green), mitochondria (Mito Deep Red, red) and overlay images (Merge) are shown. Graph: quantitative analysis of the colocalization of ER and mitochondria (% of mitochondrial volume in contact with ER). % of ER-mitochondria contact sites \pm SEM is presented in Supplementary Table S11. (a-b) Data are representative of three independent experiments. (*) $P \geq 0.001$, (**) $P < 0.001$ vs Control.

Figure 7 Mitochondrial Ca²⁺ overload is implicated in the modulation of cellular bioenergetics and mitochondrial dysfunction. (a, b) Total ATP level in SDHA_{R554W} mutated fibroblasts and in control fibroblasts left untreated (Control) or treated with Atpenin A5 as in Figure 1a (a) and in SH-SY5Y cells left untreated (Control) or treated as in Figure 1b

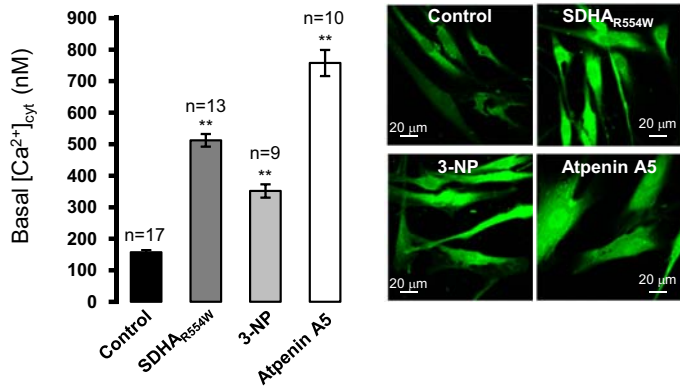
(b) in the presence or not of 10 mM 2-deoxy-D-Glucose (2-DG). % of total ATP vs Control \pm SEM and number of experiments are represented in Supplementary Table S12. (c) Total ATP level in SDHA_{R554W} mutated fibroblasts and in control fibroblasts left untreated (Control) or treated with 100 nM Atpenin A5 in the presence or not of 5 μ M BAPTA, AM for 20 h. % of total ATP vs Control \pm SEM and number of experiments are represented in Supplementary Table S13. (d) $\Delta\psi_{mit}$ analyses in control and SDHA_{R554W} fibroblasts left untreated or treated with BAPTA, AM as in (d). % of TMRM intensity vs Control \pm SEM and number of experiments are represented in Supplementary Table S14. (e) Mitochondrial superoxide content quantification performed as in Figure 1c in control and SDHA_{R554W} fibroblasts left untreated or treated with BAPTA-AM as in (d). The mean of MitoSOX intensity in % vs Control \pm SEM and number of experiments are represented in Supplementary Table S15. (d-e) Representative images are shown. (a-e) Data are representative of three independent experiments. (*) $P \geq 0.001$, (**) $P < 0.001$ (ns) non significant vs Control or vs untreated conditions (see Supplementary Tables S13-15).

Figure 8 Schematic model representing subcellular Ca²⁺ deregulation, mitochondrial dysfunction and bioenergetics outcomes upon Complex II mutation or inhibition.

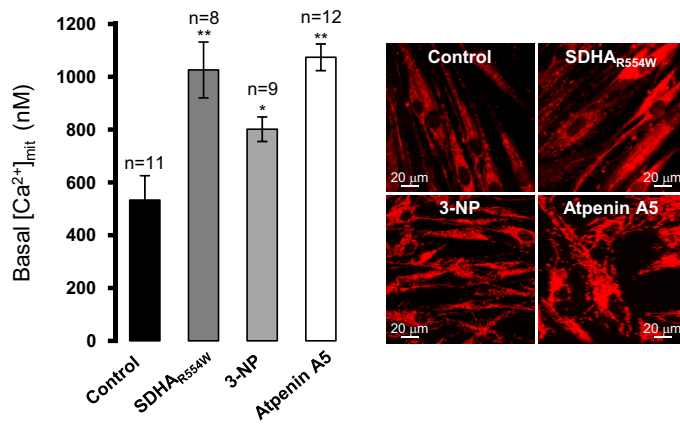
Complex II deficiency induces mitochondrial function alteration (reduced $\Delta\psi_{mit}$ and $[ATP]_{mit}$ and increased $[O_2^{\cdot-}]$), and subcellular Ca²⁺ deregulation. The increased $[Ca^{2+}]_{cyt}$ is mediated by: i) increased ER Ca²⁺ leak; and ii) degradation of PMCA and SERCA2b. Mitochondrial Ca²⁺ overload is facilitated by mitochondrial movement inhibition and increased ER-mitochondria contact sites. This leads on the one hand to mitochondrial Ca²⁺ overload and on the other hand to glycolysis-dependent ATP production. RCC: respiratory chain complexes. CLC: Ca²⁺ leak channels. U: uniporter.



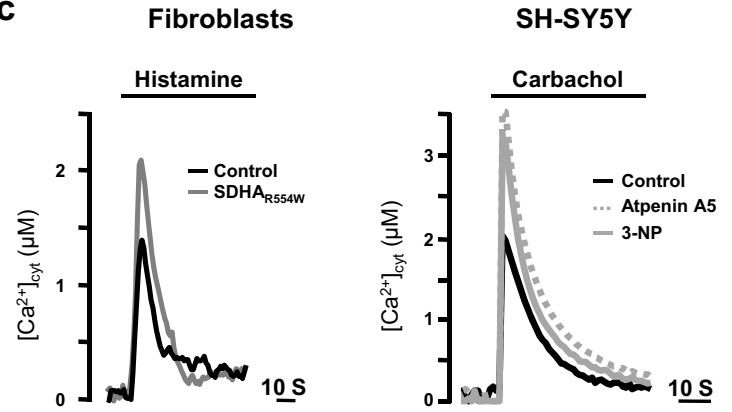
a



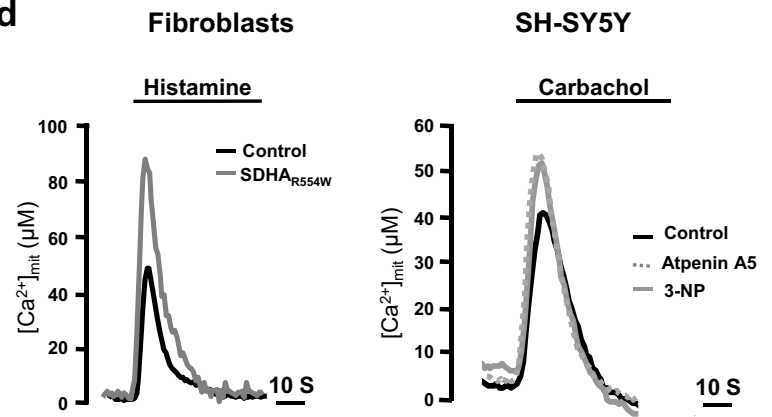
b



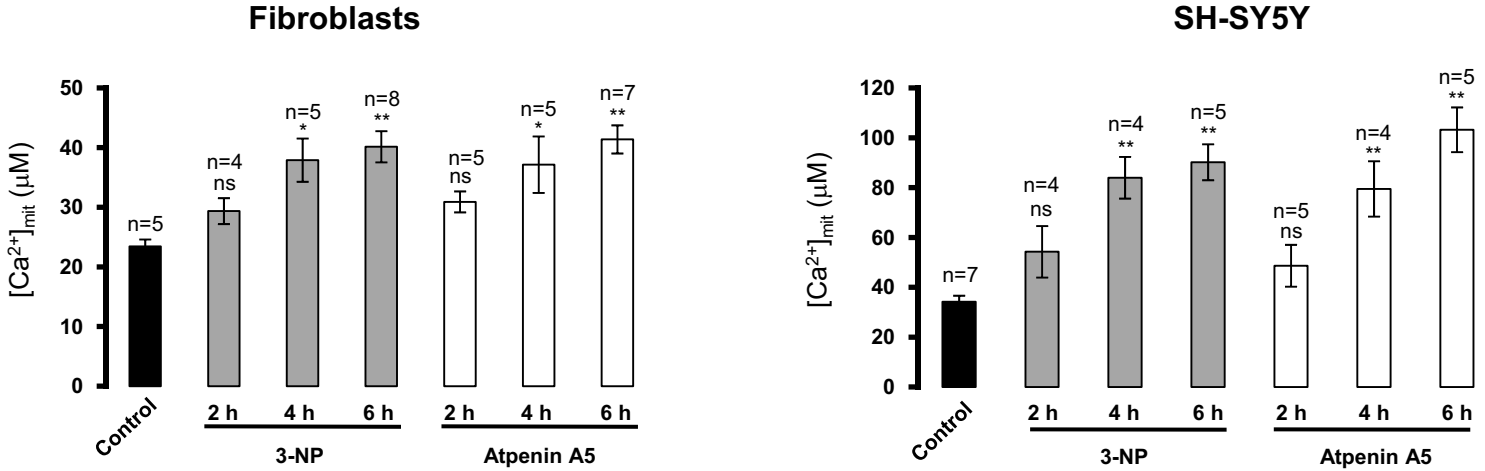
c



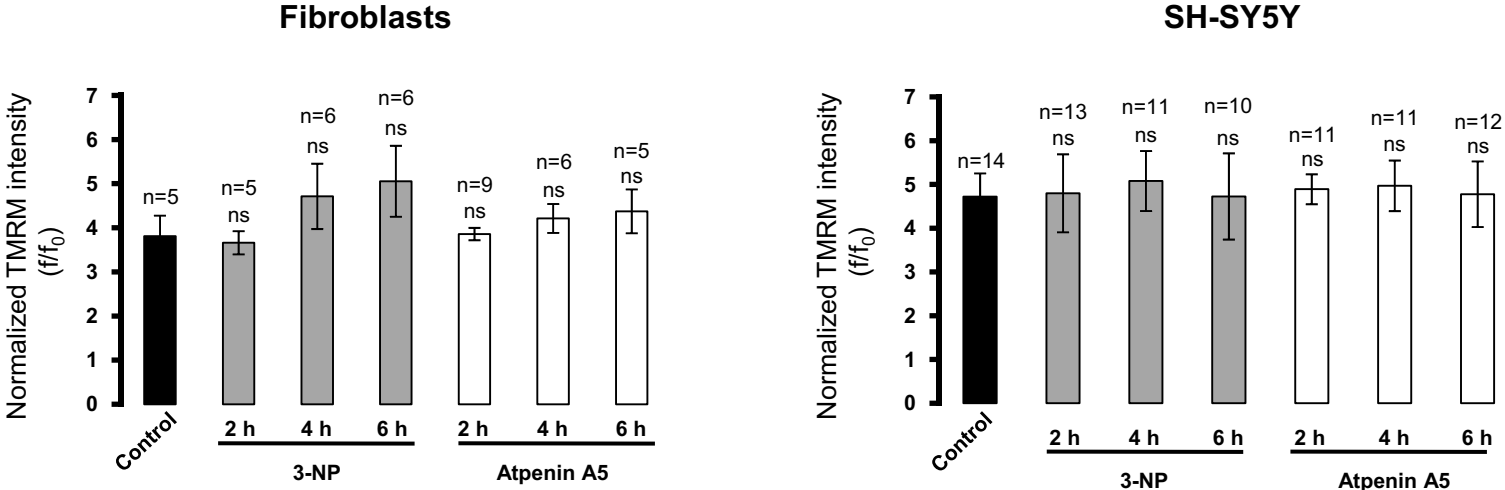
d

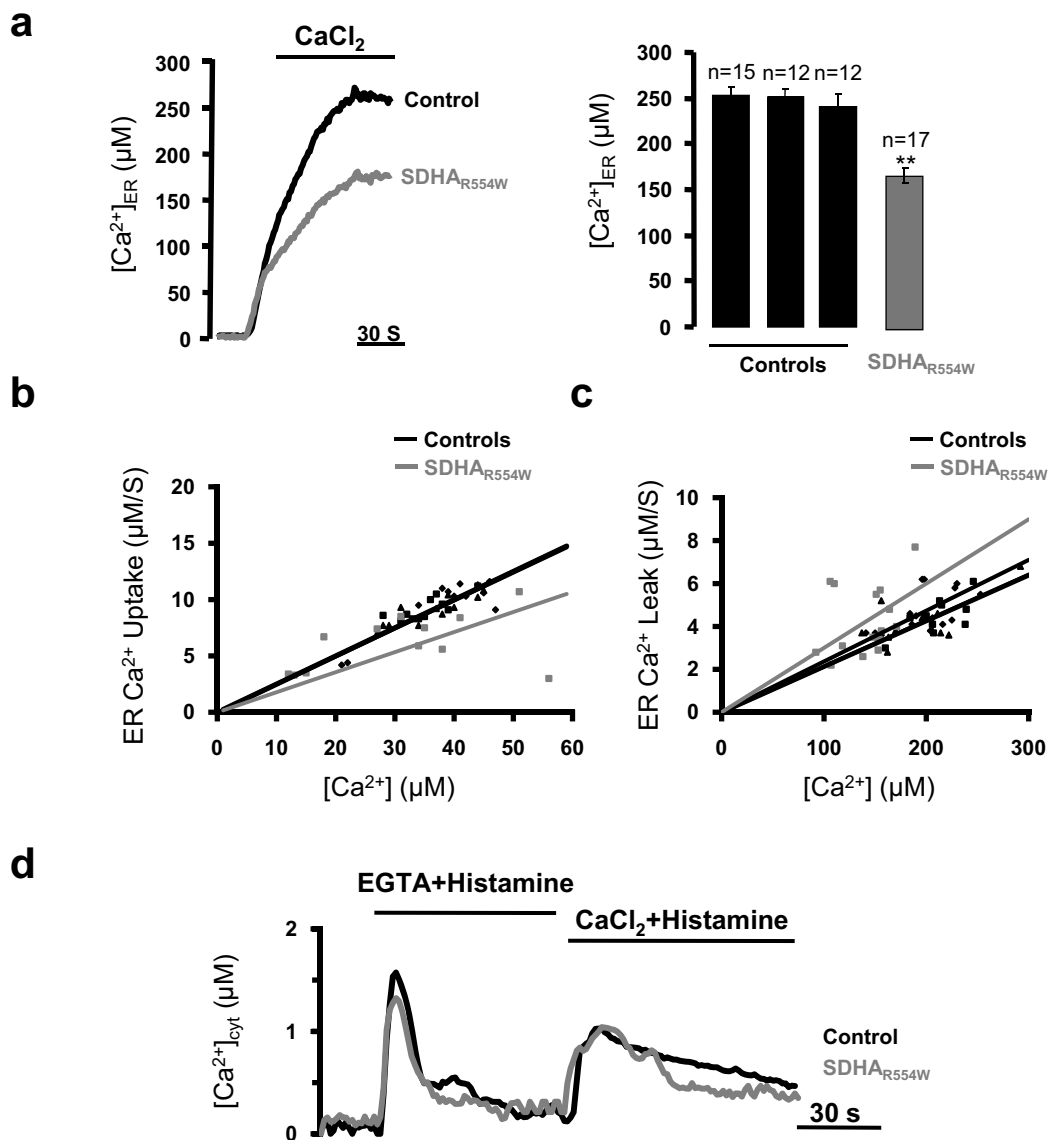


a

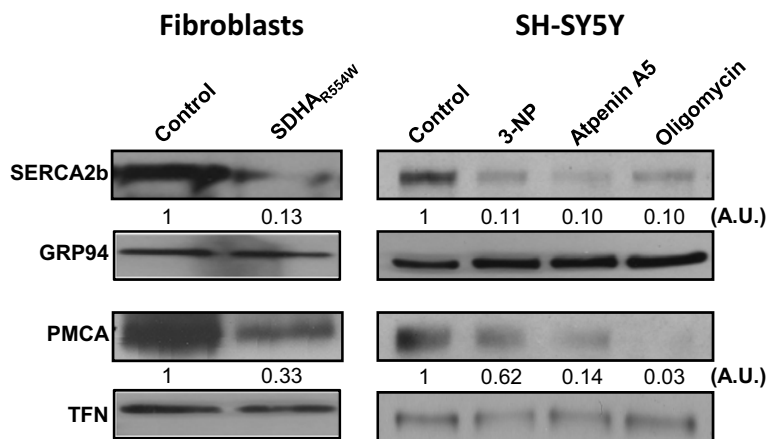


b

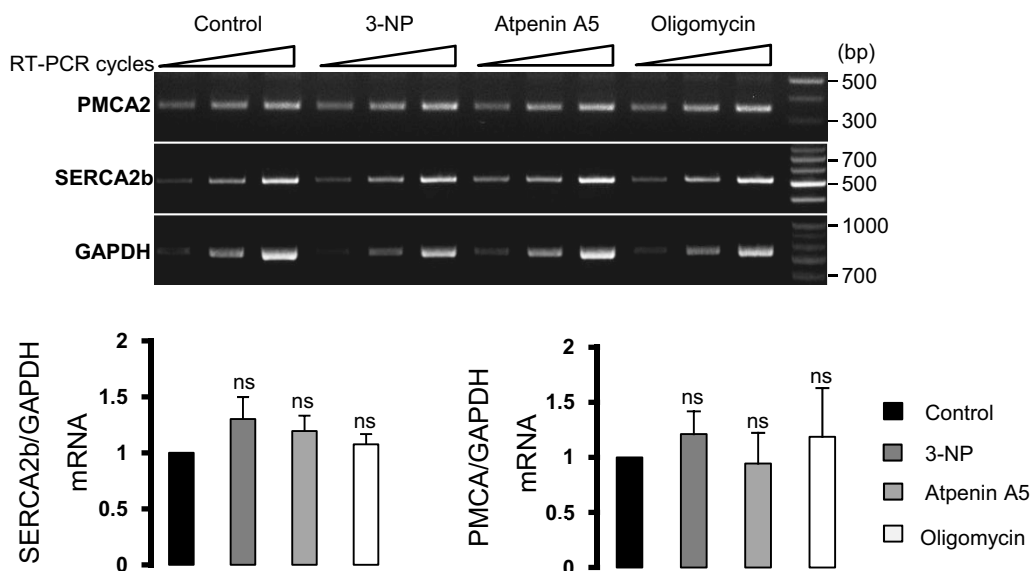




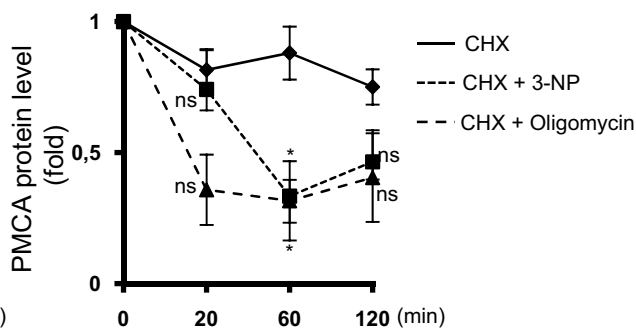
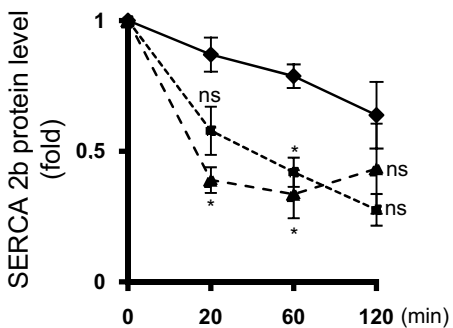
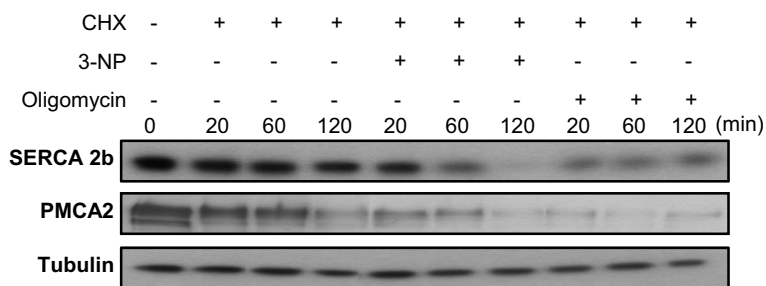
a



b



c



d

